

## VERTICAL SHEARING INSTABILITIES IN RADially SHEARING DISKS: THE DUSTIEST LAYERS OF THE PROTOPLANETARY NEBULA

E. CHIANG<sup>1</sup>

Accepted to *ApJ* Nov 26, 2007.

### ABSTRACT

Gravitational instability of a vertically thin, dusty sheet near the midplane of a protoplanetary disk has long been proposed as a way of forming planetesimals. Before Roche densities can be achieved, however, the dust-rich layer, sandwiched from above and below by more slowly rotating dust-poor gas, threatens to overturn and mix by the Kelvin-Helmholtz instability (KHI). Whether such a threat is real has never been demonstrated: the Richardson criterion for the KHI is derived for 2-D Cartesian shear flow and does not account for rotational forces. Here we present 3-D numerical simulations of gas-dust mixtures in a shearing box, accounting for the full suite of disk-related forces: the Coriolis and centrifugal forces, and radial tidal gravity. Dust particles are assumed small enough to be perfectly entrained in gas; the two fluids share the same velocity field but obey separate continuity equations. We find that the Richardson number  $Ri$  does not alone determine stability. The critical value of  $Ri$  below which the dust layer overturns and mixes depends on the height-integrated metallicity  $\Sigma_d/\Sigma_g$  (surface density ratio of dust to gas). Nevertheless, for  $\Sigma_d/\Sigma_g$  between one and five times solar, the critical  $Ri$  is nearly constant at  $\sim 0.1$ . Keplerian radial shear stabilizes those modes that would otherwise disrupt the layer at large  $Ri$ . If the height-integrated metallicity is at least  $\sim 5$  times greater than the solar value of 0.01, then midplane dust densities can approach Roche densities. Such an environment might be expected to produce gas giant planets having similarly super-solar metallicities.

*Subject headings:* hydrodynamics — instabilities — planets and satellites: formation — planetary systems: protoplanetary disks — turbulence

### 1. INTRODUCTION

How do dust grains, known to permeate disks surrounding young stars, assemble into planets? One proposed stage of growth involves gravitational instability of a dust-rich layer at the disk midplane (Safronov 1969; Goldreich & Ward 1973). If dust grains are free to settle vertically out of gas, midplane dust densities eventually exceed Roche densities, and dust particles can begin to aggregate by self-gravity.

An objection to this means of forming planetesimals is that vertical velocities of gas may be too high for dust to settle (Weidenschilling 1980). Even apart from turbulence intrinsic to gas (e.g., turbulence driven by the magneto-rotational instability), dust layers that are too vertically thin can suffer from the Kelvin-Helmholtz instability (KHI). The KHI threatens to manifest because dust-rich gas at the midplane rotates at a rate different from that of dust-poor gas at higher altitude. Dust-poor gas experiences greater acceleration from a background radial pressure gradient, and so its rotation velocity in centrifugal balance must deviate more strongly from the Keplerian value.<sup>2</sup> The deviation is smaller for gas laden with dust, since dust adds inertia but contributes no pressure. Usually it is assumed that the background radial pressure gradient  $\partial P/\partial r < 0$  so that the vertical shear in the rotation velocity  $\partial v_\phi/\partial z < 0$ .

Whether the disk is KH-unstable is commonly assessed using the Richardson number (Chandrasekhar 1961, page 491):

$$Ri \equiv \frac{(g/\rho)\partial\rho/\partial z}{(\partial v_\phi/\partial z)^2}$$

where  $g$  is the vertical gravitational acceleration and  $\rho$  is the total mass density. In the limit that perturbations are incompressible, the numerator is the square of the Brunt-Väisälä frequency of buoyant oscillations, while the denominator is the square of the vertical shearing rate. The Richardson number measures the amount of work required to overturn fluid elements that are originally in hydrostatic equilibrium, against the amount of free kinetic energy available in the background shear. For purely Cartesian flow (no rotational forces),

$$Ri < Ri_{\text{crit}} = 1/4 \text{ is necessary for instability} \quad (1)$$

(Miles 1961; Howard 1961; Chandrasekhar 1961; Drazin & Reid 1981; Li et al. 2003). Despite the fact that (1) is formally not a sufficient criterion, laboratory experiments bear out its usefulness (Tritton 1988).

Electronic address: echiang@astro.berkeley.edu

<sup>1</sup> Center for Integrative Planetary Sciences, Astronomy Department, University of California at Berkeley, Berkeley, CA 94720, USA

<sup>2</sup> This deviation from purely Keplerian flow is analogous to a “thermal wind” in the geophysical literature. See Knobloch & Spruit (1986) or Chapter 1 of Pedlosky (1979).

In the case of our disk, close to the midplane,  $g = -\Omega^2 z$  arises from the tidal gravity of the star,  $z$  measures distance from the midplane,  $\Omega$  is the Keplerian angular frequency, and  $\rho = \rho_g + \rho_d$ , where  $g$  and  $d$  denote gas and dust, respectively. Moreover,  $|\partial\rho_g/\partial z| \ll |\partial\rho_d/\partial z|$  within the thin dust layers of interest to us (see §2.2). Thus throughout this paper

$$Ri = -\frac{\Omega^2 z}{\rho_d + \rho_g} \frac{\partial\rho_d/\partial z}{(\partial v_\phi/\partial z)^2}.$$

As dust settles vertically,  $\rho_d \sim \Sigma_d/z_d$  increases; the dust surface density  $\Sigma_d$  is assumed constant while the characteristic scale height  $z_d$  of dust decreases. In the limit that  $\rho_d \gg \rho_g$ ,  $Ri \propto z_d^2$ . Criterion (1) for instability therefore places a lower bound on  $z_d$  and a corresponding upper bound on  $\rho_d$ . Unfortunately, for conventional solar nebular parameters—in particular for a height-integrated solar metallicity of  $\Sigma_d/\Sigma_g = 0.01$ —the maximum of  $\rho_d$  falls short of the Roche density by 1–2 orders of magnitude (e.g., Sekiya 1998; Youdin & Shu 2002).

But is it appropriate to apply criterion (1) to a circumstellar disk where the flow is not Cartesian? One might guess that rotational forces merely modify  $Ri_{\text{crit}}$  by a factor of order unity, since the Coriolis force and the radial shear ( $d\Omega/dr$ ) operate on a timescale  $\Omega^{-1}$ —the same timescale characterizing vertical Brunt-Väisälä oscillations and the vertical shear at  $z \sim z_d$ . Yet when Coriolis forces are introduced, as in the analysis of Gómez & Ostriker (2005, hereafter GO), the stability properties of the flow change dramatically. Numerical simulations by GO, performed under the assumption that dust is perfectly entrained in gas, reveal no well-defined threshold for instability. Unstable modes are detected for  $Ri$  as high as 4, with growth rates that diminish with increasing  $Ri$  but that show no sign of vanishing (see their Figures 9 and 10). Similar results obtain in numerical simulations by Johansen, Henning, & Klahr (2006, hereafter JHK), who relax the assumption of perfect coupling between dust and gas but who, like GO, retain only Coriolis forces and ignore radial shear. For their “rocks” and “pebbles” with momentum stopping times  $10\text{--}50 \times$  shorter than  $\Omega^{-1}$ , the dust distribution evolves to one where  $Ri$  increases from  $\sim 1$  at the midplane to  $\gtrsim 10$  at higher altitude (JHK, their Figures 4 and 5).

Here we conduct numerical simulations that account for the full complement of disk-related forces. We include not only the Coriolis force but also the centrifugal force and radial tidal gravity. The latter two forces combine to produce radial shear in rotational equilibrium. Thus we investigate the stability of doubly shearing flows: vertically shearing dust layers in near-Keplerian differential rotation. We expect our results to differ from those of GO and JHK. The modes emphasized by GO have growth rates  $\lesssim 0.1\Omega$  at  $Ri \gtrsim 2$ . Keplerian differential rotation, characterized by a strain rate of  $3\Omega/2$ , should shear such modes apart before they have time to amplify.

Indeed this is the conclusion of Ishitsu & Sekiya (2003, hereafter IS), who numerically integrate the linearized equations of motion, including the full suite of disk-related forces, to compute the factors by which modes amplify. They find that amplification factors are sufficiently limited by radial shear that midplane dust-to-gas density ratios might reach values as high as  $\sim 2$  (still too low for gravitational instability, unfortunately). They restrict, however, their linear analysis to odd-parity modes for which the vertical velocity  $v_z(z) = -v_z(-z)$ . Gómez & Ostriker (2005) establish that even-parity modes grow faster and overturn the dust layer more effectively. Our simulations do not pre-select for either type of mode. Another difference between our work and IS is that we concentrate on  $Ri = \text{constant}$  flows, whereas IS employ a simple, analytically tractable dust distribution. Of course,  $Ri = \text{constant}$  is merely a plausible condition to which the dust-gas mixture might relax. One of the goals of this study is to assess whether the Richardson number is a good predictor of stability even when all disk-related forces are accounted for. Finally, the analysis of IS is linear, while our numerical simulations enable access to nonlinear phenomena.

Our numerical simulations, like those of GO, assume that dust particles are perfectly entrained in gas, i.e., we assume that grain momentum stopping times  $\ll \Omega^{-1}$ . This approximation is valid for small particles, e.g., having sizes  $\ll 1$  m at disk radius  $r = 1$  AU in a minimum-mass nebula (e.g., Weidenschilling 1977). The hydrodynamics code and initial conditions are described in §2. Results are presented in §3; there we determine  $Ri_{\text{crit}}$  for our doubly shearing flows. A summary is provided in §4.

While our entire study is rooted in the literature on the Kelvin-Helmholtz instability and its impact on planetesimal formation, and as such revolves around the Richardson criterion, it was brought to our attention by the referee that the KHI may not be the only instability afflicting the dusty midplane. Baroclinic instabilities, studied in disks by Cabot (1984), Knobloch & Spruit (1986), and Arlt & Urpin (2004) may also be relevant. These authors study baroclinity specifically in the context of a non-zero vertical shear. More generally, a baroclinic flow is one whose isobaric surfaces do not coincide with its isodensity surfaces. Our flows are baroclinic because of molecular weight gradients: dust adds to the density but not to the pressure. Baroclinic instability can strike even when the Richardson number is large. We will connect our findings to the baroclinic instability when appropriate; indeed, in §3.1 we propose that the instability discovered by GO in their simulations of non-radially-shearing disks is, in fact, the baroclinic instability discovered by Cabot (1984). And we will see in §3.2.2 that the Richardson criterion alone does not determine stability under arbitrary conditions.

## 2. METHOD

### 2.1. Dust-Gas Equations in Tight Coupling Limit

Gas and pressureless dust are two fluids obeying separate momentum equations. In an inertial frame,

$$\frac{\partial \mathbf{v}_g}{\partial t} + (\mathbf{v}_g \cdot \nabla) \mathbf{v}_g = -\nabla \Phi + \frac{\rho_d (\mathbf{v}_d - \mathbf{v}_g)}{\rho_g t_{\text{stop}}} - \frac{\nabla P}{\rho_g} \quad (2)$$

$$\frac{\partial \mathbf{v}_d}{\partial t} + (\mathbf{v}_d \cdot \nabla) \mathbf{v}_d = -\nabla \Phi - \frac{(\mathbf{v}_d - \mathbf{v}_g)}{t_{\text{stop}}} \quad (3)$$

where  $\mathbf{v}$  is velocity,  $t$  is time, and  $\Phi$  is the background potential. Terms containing  $t_{\text{stop}}$ , the momentum stopping time for dust in gas, account for how the two fluids interact frictionally.

In this paper, we work exclusively in the tight coupling limit where particles and gas have negligible relative velocity,  $|\mathbf{v}_d - \mathbf{v}_g| \ll |\mathbf{v}_g|$ . This corresponds to the case where dust particles are so small—i.e., their surface area to mass ratios are so large—that they become entrained in the gas flow over short times. By computing the difference and appropriately weighted sum of (2) and (3) (see Youdin & Goodman 2005), and taking the limit  $t_{\text{stop}} \rightarrow 0$ , we find

$$\mathbf{v}_d - \mathbf{v}_g = 0 \quad (4)$$

$$\frac{\partial \mathbf{v}}{\partial t} + (\mathbf{v} \cdot \nabla) \mathbf{v} = -\nabla \Phi - \frac{\nabla P}{\rho_p + \rho_g} \quad (5)$$

where  $\mathbf{v} = \mathbf{v}_d = \mathbf{v}_g$ .

Furthermore,

$$\Phi = -\frac{GM}{\sqrt{r^2 + z^2}} \quad (6)$$

$$P = (\gamma - 1)\varepsilon \quad (7)$$

$$\frac{\partial \varepsilon}{\partial t} + \nabla \cdot (\varepsilon \mathbf{v}) = -P \nabla \cdot \mathbf{v} \quad (8)$$

where  $G$  is the gravitational constant,  $M$  is the central stellar mass at the origin,  $\varepsilon$  is the internal energy density of gas, and  $r$  and  $z$  are the cylindrical radius and height. The gas obeys a polytropic equation of state  $P = K \rho_g^\gamma$  with constant  $K$  and  $\gamma$ . Finally, dust and gas obey separate continuity relations

$$\frac{\partial \rho_g}{\partial t} + \nabla \cdot (\rho_g \mathbf{v}) = 0 \quad (9)$$

$$\frac{\partial \rho_d}{\partial t} + \nabla \cdot (\rho_d \mathbf{v}) = 0. \quad (10)$$

Equations (5)–(10) are the ones we solve in this paper, in the shearing box approximation (Goldreich & Lynden-Bell 1965; Hawley, Gammie, & Balbus 1995; §2.2). They contain the same content as equations (2)–(6) of GO.

In the tightly coupled limit, a fluid parcel does not change its dust-to-gas ratio in a Lagrangian sense:  $d(\rho_d/\rho_g)/dt = 0$ , where  $d/dt$  is the convective derivative. Particles cannot slip away from gas, and so we cannot expect our simulated flows to relax, from arbitrary initial conditions, into a unique, steady state of marginal stability (if such a state actually exists). In reality, such relaxation occurs over the time it takes dust to settle vertically relative to gas. Vertical settling times are measured in Myrs for micron-sized particles (or  $\sim 10^2$  yr for centimeter-sized particles) in a minimum-mass nebula. Nevertheless, our equations do permit dust-rich parcels to settle toward the midplane if their weight cannot be supported in vertical hydrostatic equilibrium. We are able to evolve dust-gas mixtures over dynamical times, measured in orbital periods, provided  $t_{\text{stop}}$  is still shorter. Our simulations can thus determine whether a given set of equilibrium conditions is dynamically stable. We now specify these equilibrium initial conditions.

## 2.2. Initial Conditions: Constant $Ri$ Flows

Call  $r_0$  and  $\phi_0 = \Omega_0 t$  the radius and azimuth of a test particle moving on a circular orbit, where  $\Omega_0 = \sqrt{GM/r_0^3}$ . Shifting to axes centered on the test particle and rotating at  $\Omega_0$ , we trade the usual cylindrical coordinates  $(r, \phi, z)$  for their shearing sheet counterparts  $(x, y, z)$ :  $x \equiv r - r_0$ ,  $|x| \ll r_0$ ,  $y = (\phi - \phi_0)r_0$ ,  $|y| \ll r_0$ , and  $|z| \ll r_0$ . In this rotating frame, the momentum equation (5) reads

$$\frac{\partial v_x}{\partial t} + v_i \frac{\partial v_x}{\partial x_i} = \frac{-1}{\rho_g + \rho_d} \frac{\partial P}{\partial x} + 2\Omega_0 v_y + 2q\Omega_0^2 x \quad (11)$$

$$\frac{\partial v_y}{\partial t} + v_i \frac{\partial v_y}{\partial x_i} = \frac{-1}{\rho_g + \rho_d} \frac{\partial P}{\partial y} - 2\Omega_0 v_x \quad (12)$$

$$\frac{\partial v_z}{\partial t} + v_i \frac{\partial v_z}{\partial x_i} = \frac{-1}{\rho_g + \rho_d} \frac{\partial P}{\partial z} - \Omega_0^2 z \quad (13)$$

where  $i = (1, 2, 3)$ ,  $(x_1, x_2, x_3) = (x, y, z)$ ,  $(v_1, v_2, v_3) = (v_x, v_y, v_z)$ , and curvature terms of order  $v^2/r$  are dropped, following the shearing sheet approximation. We introduce the variable  $q = -d \ln \Omega / d \ln r$  in (11) because in our simulations we experiment with  $q = 0$  (zero radial shear) to connect to GO. For the full problem with a point-mass potential,  $q = 3/2$ .

In rotational equilibrium, equation (11) for radial momentum balance gives

$$v_y = -q\Omega_0 x + \frac{1}{2\Omega_0(\rho_d + \rho_g)} \frac{\partial P}{\partial x}. \quad (14)$$

Initially,  $\partial P / \partial x = (\partial P / \partial r)_{t=0}$  reflects how the background nebular pressure changes radially on scales of  $r$ . We express  $(\partial P / \partial r)_{t=0}$  in terms of a model input parameter,  $v_{\max}$ :

$$\left( \frac{\partial P}{\partial r} \right)_{t=0} \equiv -2\rho_g(z, t=0)v_{\max}\Omega_0. \quad (15)$$

The velocity  $v_{\max}$  represents the difference between the Keplerian rotation rate and the sub-Keplerian rotation rate of pressure-supported gas; it measures the maximum possible difference in rotational velocity between the dust-rich midplane and dust-free gas at higher altitude. For typical nebular parameters, it is approximately 20 m/s and nearly constant with  $r$ .

Further defining the local dust-to-gas ratio  $\mu \equiv \rho_d / \rho_g$ , we rewrite (14) as

$$v_y(x, z, t=0) = -q\Omega_0 x - \frac{v_{\max}}{1 + \mu(z)}. \quad (16)$$

In each of our simulations, we hold  $v_{\max}$  fixed for simplicity. Then the vertical shear,  $\partial v_y / \partial z$ , is non-zero only when  $\partial \mu / \partial z$  is non-zero. Because  $\mu$  varies rapidly with  $z$  for the vertically thin dust layers of interest to us, approximating  $v_{\max}$  as constant introduces negligible error.

All our simulations investigate the stability of constant  $Ri$  flows. The condition  $Ri = \text{constant}$  yields  $\mu(z)$ :

$$\begin{aligned} Ri &= -\frac{\Omega_0^2 z}{\rho_d + \rho_g} \frac{\partial \rho_d / \partial z}{(\partial v_y / \partial z)^2} \\ &= -\frac{\Omega_0^2}{v_{\max}^2} \frac{(1 + \mu)^3 z}{\partial \mu / \partial z} \end{aligned}$$

which integrates to

$$\mu(z) = \left[ \frac{1}{1/(1 + \mu_0)^2 + (z/z_d)^2} \right]^{1/2} - 1 \quad (17)$$

where  $\mu_0 \equiv \mu(z=0)$  is a model input parameter and

$$z_d \equiv \frac{Ri^{1/2} v_{\max}}{\Omega_0}$$

is a characteristic dust height. Equation (17) implies that dust extends to a maximum height

$$z_{\max} = z_d \frac{\mu_0^{1/2} (2 + \mu_0)^{1/2}}{1 + \mu_0}.$$

Finally, vertical hydrostatic equilibrium gives  $\rho_g(z)$ :

$$\frac{1}{\rho_g + \rho_d} \frac{\partial P}{\partial z} = -\Omega_0^2 z \quad (18)$$

which, using (17), can be solved analytically for  $\rho_g$ . The expressions, which differ for  $0 \leq z < z_{\max}$  and  $z > z_{\max}$ , are not especially illuminating and so we omit them here.

Self-gravity is ignored. Its neglect is justified for densities less than the Roche density,  $(\rho_g + \rho_d) \ll M / (2\pi r^3)$ . Equivalently, for standard nebular parameters, we are restricted to  $\mu \ll 30$ . Sekiya (1998; see also Youdin & Shu 2002) relaxes this condition and accounts for vertical self-gravity in computing the Richardson number.

Figure 1 shows profiles for  $\rho_g(z)$  and  $\rho_d(z)$ , for normalized (code) parameters of  $\rho_{g0} = \rho_g(z=0) = 1$ ,  $K = 1$ ,  $\gamma = 5/3$ ,  $\Omega_0 = 1$ ,  $Ri = 1$ ,  $\mu_0 = 0.475$ , and  $v_{\max}/c_{s0} = 0.05$ , where  $c_{s0} = \sqrt{\gamma K \rho_{g0}^{\gamma-1}} = 1.3$  is the sound speed at the midplane. These parameter choices imply a height-integrated dust-to-gas surface density ratio (height-integrated metallicity) of  $\Sigma_d / \Sigma_g = 0.01$ , the nominal solar value. We vary  $Ri$  and  $\mu_0$  from simulation to simulation. Note that our choice of  $v_{\max}/c_{s0} = 0.05$  is a factor of 2 smaller than that of GO because we prefer to use gas temperatures

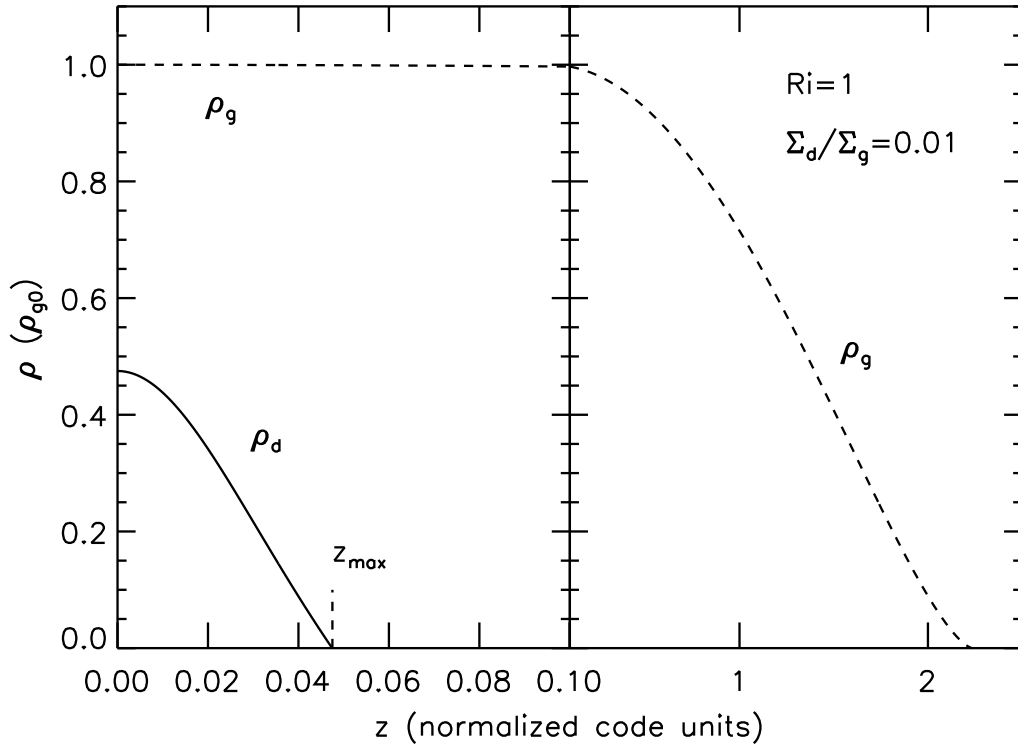


FIG. 1.— Dust and gas vertical density profiles, computed for constant  $Ri = 1$  and vertical hydrostatic equilibrium. Disk self-gravity is neglected (cf. Sekiya 1998). Note the change in horizontal scale between the two panels. The dust density  $\rho_d$  is zero at  $z = z_{\max}$ . Typically our simulations span  $z = \pm z_{\max}$ ; the gas density  $\rho_g$  is practically constant on these scales.

characterizing passive disks (see, e.g., Chiang et al. 2001) rather than the hotter temperatures of the Hayashi (1981) nebula. Disk gas must be fairly passive, i.e., not heated by turbulent dissipation, for dust to settle into the thin layers of interest here (see Appendix B of Youdin & Chiang 2004 for estimates of the degree of turbulence permitted). A factor of 2 decrease in  $v_{\max}/c_{s0}$  produces a factor of 2 increase in the central concentration  $\mu_0$ , at fixed  $Ri$  and fixed  $\Sigma_d/\Sigma_g$ . Figure 2 is analogous to Figure 1, except that  $Ri = 0.125$  and  $\mu_0 = 1.31$  (so that again  $\Sigma_d/\Sigma_g = 0.01$ ). Figure 3 is analogous to Figure 2, except that  $\mu_0 = 23.3$ , so that  $\Sigma_d/\Sigma_g = 0.05$  (the height-integrated metallicity is super-solar by a factor of 5).

To summarize this subsection, our equilibrium initial conditions specify  $v_y$  through (16),  $\mu \equiv \rho_d/\rho_g$  through (17), and  $\rho_g$  through analytic solution of (18). Initially,  $v_x = v_z = 0$ , and  $\rho_g$  and  $\rho_d$  are constant with  $x$  and  $y$ . The primary input parameters are  $Ri$  and  $\mu_0$ ; we hold  $v_{\max}/c_{s0} = 0.05$  fixed for all runs.

### 2.3. Code

We employ the hydrodynamics code ZEUS (Stone & Norman 1992), a version of which was kindly given to us by Dr. Bryan Johnson. Because we are interested in flows that shear both in radius ( $\partial v_y/\partial x$ ) and height ( $\partial v_y/\partial z$ ), the simulations are necessarily three-dimensional. We adopt the usual shearing box (e.g., Hawley, Gammie, & Balbus 1995), with shearing periodic boundary conditions in  $x$ , periodic boundary conditions in  $y$ , and closed boundary conditions in  $z$ .

Three modifications are made to the code. The first is the addition of another fluid, dust, which is transported according to its own continuity equation (10), but otherwise has the same velocity as that of gas. The second modification is to the pressure gradient source term:  $\nabla P/\rho_g \rightarrow \nabla P/(\rho_g + \rho_d)$ , in accordance with (2.2). The final change is to introduce an extra source term for the “large-scale” radial pressure gradient, distinct from the just mentioned “local” pressure gradient. That is, equation (11) for the  $x$ -momentum is revised to read

$$\frac{\partial v_x}{\partial t} + v_i \frac{\partial v_x}{\partial x_i} = \frac{-1}{\rho_g + \rho_d} \frac{\partial P}{\partial x} + 2\Omega_0 v_y + 2q\Omega_0^2 x - \frac{1}{\rho_g + \rho_d} \left( \frac{\partial P}{\partial r} \right)_{t=0}. \quad (19)$$

The extra source term  $(\partial P/\partial r)_{t=0}$  is given by (15). It accounts for how the pressure changes over radial lengthscales of  $r$ , and is held fixed for each simulation. Its inclusion is necessary to have dust-rich gas rotate faster than dust-poor

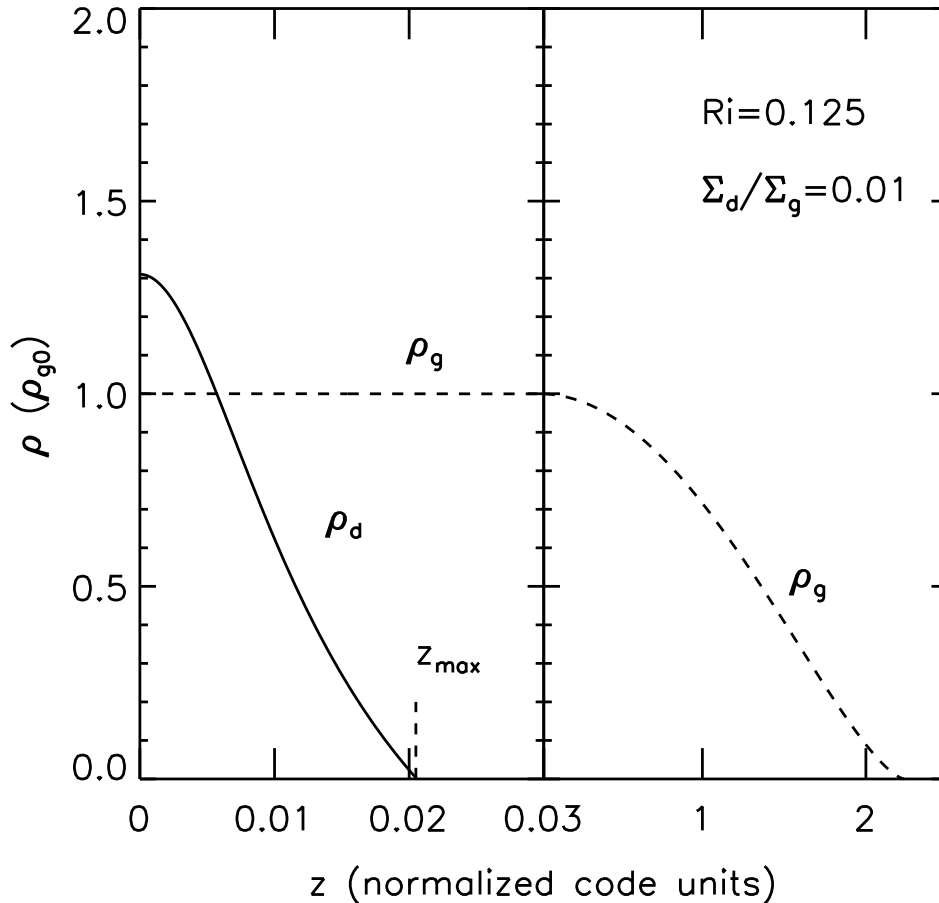


FIG. 2.— Same as Figure 1, but for  $Ri = 0.125$ .

gas initially, i.e., to drive the vertical shear. But because our simulations use a shearing box—in other words, because they are local—we cannot follow the evolution of this large-scale gradient. A self-consistent treatment would require us to model the disk globally. Our use of an external, constant, radial pressure gradient is the same device employed by GO. The error introduced is negligible insofar as changes in pressure over lengthscales of  $r$  occur over timescales much longer than the dynamical timescales which concern us here.

In short, the modified code solves equations (7)–(10), (12), (13), and (19). Initial conditions for the code are given above in §2.2. The equilibrium state is perturbed by adding a random velocity to each grid cell. The perturbation velocity points in a random direction from cell to cell. For our main set of runs, the magnitude of the perturbation in each cell is drawn at random from a uniform distribution that extends from zero to  $10^{-3}c_{s0}$  (for comparison, the maximum vertical shearing velocity is about  $v_{\max} = 0.05c_{s0}$ ). Several auxiliary runs use much smaller or more spatially limited initial perturbations; these are described in §3.2.1 and produce the same outcomes as our main simulations.

Our standard box dimensions are  $L_x = L_y = 8z_{\max}$  and  $L_z = 4z_{\max}$ , and the corresponding number of grid cells is  $(N_x, N_y, N_z) = (64, 64, 32)$ . The duration of each simulation is at least  $t_f = 20\Omega_0^{-1}$ . Run parameters are contained in Tables 1 and 2, and are justified in §3.

Including the von Neumann & Richtmyer (1950) artificial viscosity makes little difference to our results—not surprisingly since our flows are highly subsonic ( $v_{\max}/c_{s0} = 0.05$ ). Therefore the simulations reported in this paper have no artificially imposed viscosity apart from the unavoidable numerical kind.

### 3. RESULTS

#### 3.1. Coriolis Only: $q = 0$

To test our code, we repeat the experiments of GO. The Coriolis acceleration is retained but the radial shear is suppressed by setting  $q = 10^{-6}$  in the code. Effectively, this converts shearing boundary conditions in  $x$  to periodic

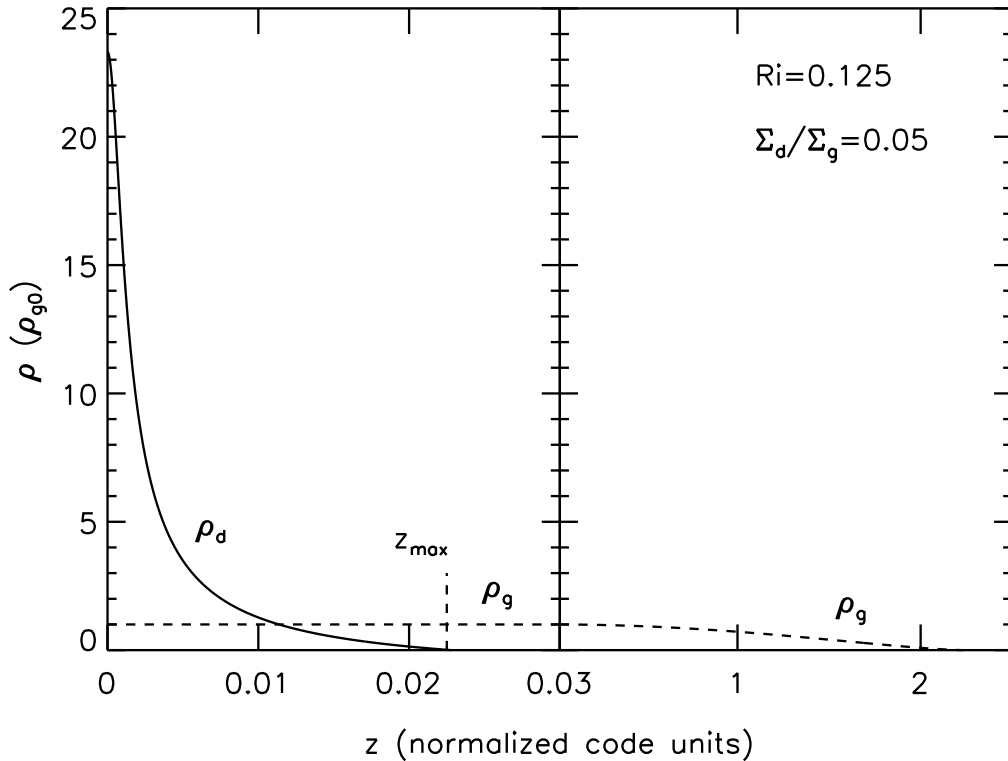


FIG. 3.— Same as Figure 2, but for a super-solar metallicity  $\Sigma_d/\Sigma_g = 0.05$ . The Richardson number, 0.125, is about the lowest it can be without the dust layer turning over for this metallicity (see Run S8 of Table 2). The midplane dust density, more than 20 times higher than the local gas density, is sufficiently high that dust self-gravity can be dynamically important. Ways of achieving  $\Sigma_d/\Sigma_g = 0.05$  are mentioned in §4.

boundary conditions. It also eliminates the contribution,  $2q\Omega_0^2 x$ , to  $dv_x/dt$  from the centrifugal force and tidal gravity. Since the resultant flows have no structure in  $x$ , we reduce  $N_x$  to 2 and  $L_x$  to  $0.25z_{\max}$ .

Table 1 lists the run parameters. The main parameter varied from run to run is  $Ri$ ; the central concentration  $\mu_0$  is adjusted in tandem to keep  $\Sigma_d/\Sigma_g = 0.01$  fixed for all runs (this restriction to solar metallicity is relaxed for the fully shearing runs of §3.2). Following GO, we diagnose the flow by Fourier analyzing  $v_z$  in the  $y$ -direction at fixed  $x$ ,  $z$ , and  $t$ . We then inspect how the Fourier amplitudes change with time. We are interested in those modes whose  $y$ -wavelengths  $\lambda_y$  are comparable to the dust layer thickness  $z_{\max}$ , as shorter wavelength modes cannot overturn the layer and longer wavelength modes grow more slowly. We are able to measure the exponential growth rates  $\omega_I$  of several modes whose  $\lambda_y$ 's range from  $\sim 8/15$  to  $\sim 8/3$  of  $z_{\max}$ .<sup>3</sup> Figure 4 displays the Fourier amplitudes versus time for the  $\lambda_y/z_{\max} = 8/7$  mode, in simulations of varying  $Ri$ . While the growth rate  $\omega_I$  of this mode decreases with increasing  $Ri$ , growth is still reliably detected for  $Ri$  as high as 16, a value  $64\times$  greater than the canonical threshold of  $1/4$ . Our measured growth rates are similar to those reported by GO (see their Figure 10).

Runs C1a–C1f test the sensitivity of our results to simulation box size and spatial resolution. Doubling the box height  $L_z$  to  $8z_{\max}$  at fixed resolution produces negligible change in measured growth rates (C1a vs. C1). Doubling the vertical resolution by doubling  $N_z$  at fixed  $L_z$  increases mode growth rates by  $\sim 10\%$  (C1b vs. C1). Changes in  $\omega_I$  of order 10% are also produced by varying the azimuthal parameters  $L_y$  and  $N_y$  by factors of 2 (C1c–C1f). We conclude that our standard box size  $(L_y, L_z) = (8, 4)z_{\max}$  and resolution  $(N_y, N_z) = (64, 32)$  adequately balance the need for accuracy with the need for computational speed.

Table 1 and Figure 4 suggest that when only the Coriolis force is included, and radial shear is omitted, dust layers characterized by surprisingly large values for  $Ri$  will eventually overturn and mix. This conclusion is supported by Figure 5, which displays snapshots of a high-resolution  $(N_y, N_z) = (128, 64)$  run for which  $Ri = 4$ . Despite  $Ri$  being  $16\times$  greater than the traditional critical value of  $1/4$ , the dust layer is clearly unstable. The fastest growing mode has  $\lambda_y/z_{\max} \approx 8/5$  and overturns the layer by  $t \approx 100\Omega_0^{-1}$ . All these results agree with those of GO.

We suspect that the instability discussed in this section, and simulated first by GO, is a baroclinic instability afflicting

<sup>3</sup> Periodic boundary conditions in  $y$  imply that the only modes present are those for which the simulation box fits an integral number of wavelengths. The standard box length is  $L_y = 8z_{\max}$ .

TABLE 1  
CORIOLIS ONLY ( $q = 0$ ) SIMULATIONS

Name	$N_x$	$L_x$ ( $z_{\max}$ )	$N_y$	$L_y$ ( $z_{\max}$ )	$N_z$	$L_z$ ( $z_{\max}$ )	$Ri$	$\mu_0$	$\Sigma_d/\Sigma_g$	$t_f$ ( $\Omega_0^{-1}$ )	$\lambda_y^a$ ( $z_{\max}$ )	$\omega_I$ ( $\Omega_0$ )
C1a <sup>b</sup>	2	0.25	64	8	64	8	0.25	0.903	0.01	20	8/3	0.334
C1b	"	"	64	8	64	4	"	"	"	"	8/3	0.371
C1c	"	"	64	16/3	32	4	"	"	"	"	8/3	0.352
C1d	"	"	32	8/3	"	"	"	"	"	"	8/3	0.368
C1e	"	"	32	3	"	"	"	"	"	"	3	0.339
C1f	"	"	64	7	"	"	"	"	"	"	7/3	0.336
C1	"	"	64	8	32	4	"	"	"	40	8/3	0.332
											8/5	0.303
											8/7	0.342
C2	"	"	"	"	"	"	1	0.475	"	"	8/3	NA <sup>c</sup>
											8/5	0.165
											8/7	0.203
C3	"	"	"	"	"	"	1.581	0.391	"	"	8/3	NA
											8/5	0.148
											8/7	0.171
C4	"	"	"	"	"	"	2.5	0.324	"	"	8/3	NA
											8/5	0.088
											8/7	0.142
C5	"	"	"	"	"	"	3.952	0.270	"	"	8/3	NA
											8/5	0.084
											8/7	0.125
C6	"	"	"	"	"	"	6.248	0.226	"	"	8/3	NA
											8/5	NA
											8/7	0.093
C7	"	"	"	"	"	"	9.878	0.190	"	"	8/3	NA
											8/5	NA
											8/7	0.078
C8	"	"	"	"	"	"	15.62	0.161	"	"	8/3	NA
											8/5	NA
											8/7	0.062

<sup>a</sup> Wavelength of a sampled mode. Other modes exist and were measured that are not listed here. In runs C1a–C1f, the listed mode is the strongest mode. <sup>b</sup> Runs C1a–C1f experiment with the size and spatial resolution of the simulation box. <sup>c</sup> NA denotes a mode whose Fourier amplitude does not grow smoothly and exponentially over the duration of the simulation. In most cases the amplitude either remains roughly constant or decreases.

$q = 0$  disks. Cabot (1984) finds that baroclinic,  $q = 0$  disks are linearly unstable to non-axisymmetric perturbations; that the “baroclinic instability draws its energy from radial excursions by fluid elements” (radial excursions made possible by the Coriolis force); and that maximum growth rates  $\omega_I$  are of order the maximum vertical shearing frequency  $\max |\partial v_y / \partial z|$  (see his Table 1 and the discussion following his equation 22b). For our dusty layers,  $\max |\partial v_y / \partial z| \approx \Omega / \sqrt{Ri}$ ; support for the inverse square-root dependence on  $Ri$  can indeed be found in Figure 4.<sup>4</sup>

Knobloch & Spruit (1986) extend the work of Cabot (1984) by restoring the effects of Keplerian shear to baroclinic disks. They find that radial shear tends to stabilize the flow to non-axisymmetric disturbances. For their particular choice for the form of  $v_y(z) \propto -z^4$ , the linear baroclinic instability is defeated when baroclinicity is small ( $|\partial v_y / \partial z| \ll \Omega$ ) and when the disk is strongly stable to thermal convection in the vertical direction. These stability requirements are usually satisfied in disks without gradients in mean molecular weight (such disks are their main concern). Knobloch & Spruit (1986) speculate that instability occurs when baroclinicity is large. In the context of their disks, large baroclinicity demands variations in specific entropy on short radial length scales  $\lesssim h$ , the vertical height of disk gas. Rapid radial variations are also required for instability by Arlt & Urpin (2004), who study axisymmetric perturbations.

But large baroclinicity can also be achieved by having a strong molecular weight gradient in the vertical direction, as exists in a highly settled dust layer. We turn now to simulating such highly baroclinic, radially shearing flows.

### 3.2. Coriolis + Radial Shear: $q = 3/2$

Having found simulation parameters ( $L_y, L_z, N_y, N_z$ ) that produce realistic results for  $q = 0$ , we use those same parameters for our radially shearing  $q = 3/2$  simulations. Since the radial wavenumber of a disturbance grows at rate  $\dot{k}_x = q\Omega_0 k_y$ , our resolution in  $x$  should be at least comparable to that in  $y$ . Our standard run parameters are  $(L_x, L_y, L_z) = (8, 8, 4)z_{\max}$  and  $(N_x, N_y, N_z) = (64, 64, 32)$ . Table 2 lists the various experiments, all of which start with  $Ri = \text{constant}$  flow as described in §2.2. Whether the dust layer turns over within the run duration is indicated

<sup>4</sup> Our shearing rates are much larger than those considered by Cabot (1984), who analyzed pure gas disks with no gradients in mean molecular weight. When  $\Sigma_d = 0$ , the maximum vertical shear is  $\max |\partial v_y / \partial z| = \xi \Omega h / r$ , where  $h \approx c_s / \Omega < r$  is the hydrostatic disk thickness and  $\xi$  is a number typically of order 0.1. The smallness of  $\xi$  arises because two effects compete and nearly cancel: both the radial gravity  $-\partial \Phi / \partial r$  and the radial pressure acceleration  $-(1/\rho)\partial P / \partial r$  decrease in magnitude with increasing height.

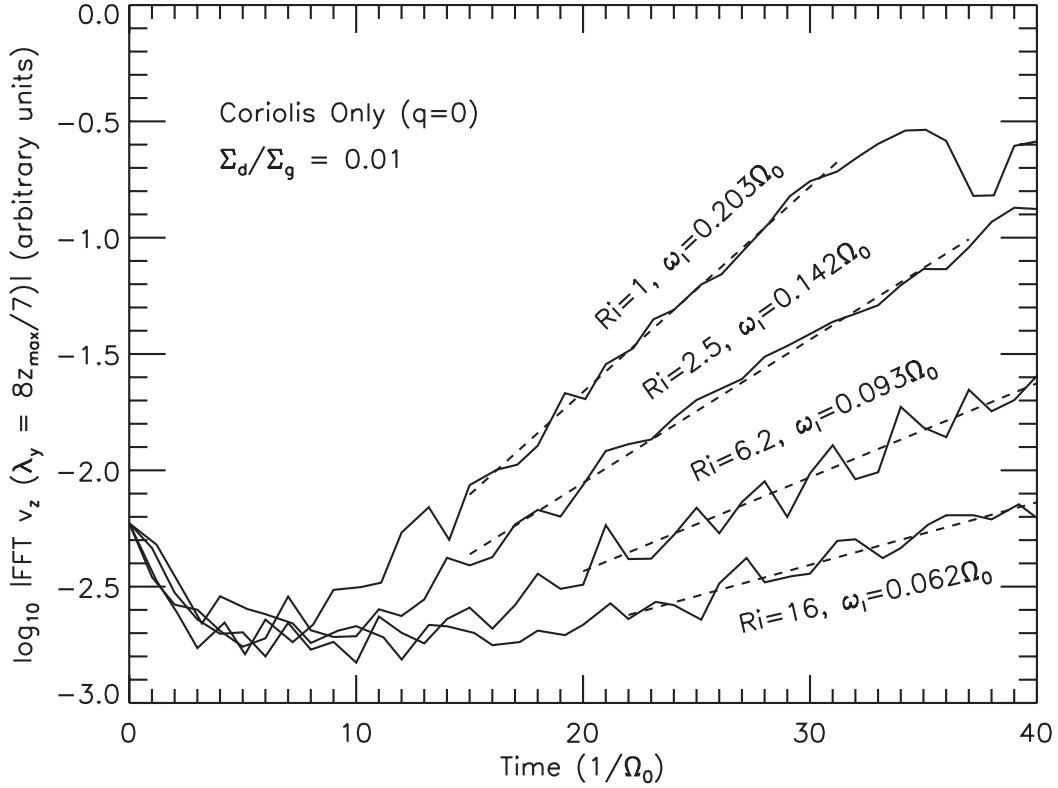


FIG. 4.— Fourier amplitudes versus time for the  $\lambda_y/z_{\max} = 8/7$  mode, in simulations of varying  $Ri$ . At fixed  $x = 0.0625z_{\max}$ , and given  $z$  and  $t$ , we compute the fast Fourier transform (FFT) of  $v_z$  in the  $y$ -direction. What is plotted at a given  $t$  is the maximum value of the FFT (for the chosen  $\lambda_y$ ) over all  $z$ . Growth rates  $\omega_I$  are the slopes of lines fitted to the linear growth phase.

TABLE 2  
FULLY SHEARING ( $q = 3/2$ ) SIMULATIONS

Name	$N_x$	$L_x$ ( $z_{\max}$ )	$N_y$	$L_y$ ( $z_{\max}$ )	$N_z$	$L_z$ ( $z_{\max}$ )	$Ri$	$\mu_0$	$\Sigma_d/\Sigma_g$	Noise <sup>a</sup> ( $c_{s0}$ )	$t_f$ ( $\Omega_0^{-1}$ )	Turns Over?
S1	64	8	64	8	32	4	0.25	0.903	0.01	$10^{-3}$	40	N <sup>b</sup>
S2	"	"	"	"	"	"	0.125	1.31	"	$10^{-3}$	100	N
S2a	128	"	128	"	64	"	"	"	"	$10^{-3}$	20	N
S3	64	8	64	8	32	4	0.0625	1.989	"	$10^{-3}$	50	Y
S3a	"	"	"	"	"	"	"	"	"	$10^{-6}$	70	Y
S4	"	"	"	"	"	"	0.03125	3.252	"	$10^{-3}$	20	Y
S4a	"	"	"	"	"	"	"	"	"	$10^{-6}$	40	Y
S5	"	"	"	"	"	"	0.25	3.57	0.03	$10^{-3}$	20	N
S6	"	"	"	"	48 <sup>c</sup>	"	0.125	6.65	"	$10^{-3}$	20	N
S7	"	"	"	"	64 <sup>c</sup>	"	0.0625	14.7	"	$10^{-3}$	20	Y
S8 <sup>d</sup>	"	"	"	"	64 <sup>c</sup>	"	0.125	23.3	0.05	$10^{-3}$	20	N
S9	"	"	"	"	32	"	0.125	0.174	0.001	$10^{-3}$	70	N
S10	"	"	"	"	"	"	0.0625	0.226	"	$10^{-3}$	70	N
S11	"	"	"	"	"	"	0.03125	0.296	"	$10^{-3}$	70	N
S12	"	"	"	"	"	"	0.01563	0.393	"	$10^{-3}$	70	Y

<sup>a</sup> Maximum initial perturbation velocity applied to each grid cell. From cell to cell, the perturbation velocity points in a random direction, and its magnitude is drawn randomly from a uniform distribution from 0 to the maximum indicated in the table. For comparison, the maximum vertical shearing velocity is about  $v_{\max} = 0.05c_{s0}$ . <sup>b</sup> For runs in which the layer does not overturn, we perform the same Fourier analysis that we do for Coriolis-only runs, and detect no growing modes at all. <sup>c</sup> Increasing  $\mu_0$  (equivalently,  $\Sigma_d/\Sigma_g$ ) at fixed  $Ri$  steepens the dust density profile  $\rho_d(z)$ , whose resolution then requires greater  $N_z$ . <sup>d</sup> We do not simulate  $Ri = 0.0625$  and  $\Sigma_d/\Sigma_g = 0.05$ , since for such parameters  $\mu_0 = 79.5$ ; dust self-gravity, which we do not account for, would be significant in this case.

in the table.

Results for  $q = 3/2$  differ dramatically from those for  $q = 0$ . Whereas instability characterizes all values of  $Ri$  for  $q = 0$ , we find that  $Ri$  must fall below a critical value,  $Ri_{\text{crit}} \approx 0.1$ , for the layer to overturn when  $q = 3/2$  and when

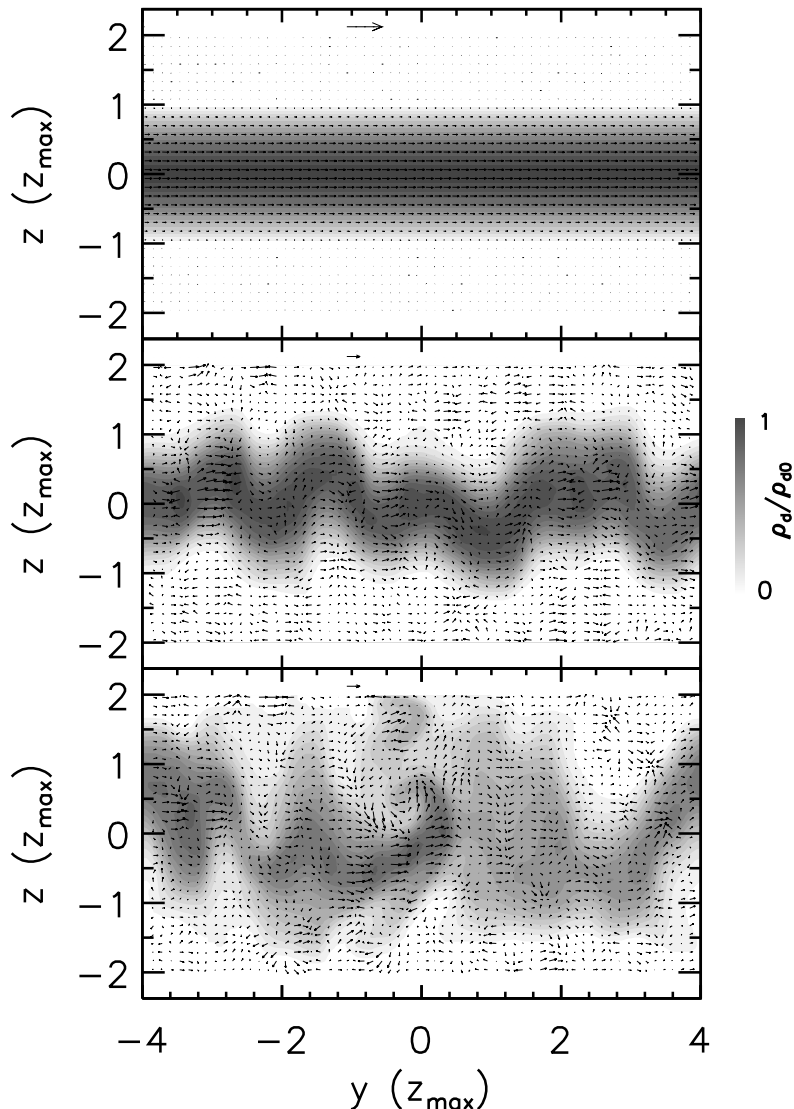


FIG. 5.— Snapshots of the  $(y, z)$  flow for  $Ri = 3.952$  and  $\mu_0 = 0.270$ , including only Coriolis forces ( $q = 0$ ), at times  $t = 0$  (top),  $t = 95\Omega_0^{-1}$  (middle), and  $t = 170\Omega_0^{-1}$  (bottom). Greyscale denotes the density of dust only, normalized to the density of dust at the midplane at  $t = 0$ . Velocity vectors are shown in the frame rotating with dust-free gas (see top panel). The lone arrow at the top of each panel gives the length of  $v_{\max}$  for that panel only. Data are based on a simulation for which  $(L_x, L_y, L_z) = (0.25, 8, 4)z_{\max}$  and  $(N_x, N_y, N_z) = (2, 128, 64)$ .

$\Sigma_d/\Sigma_g = 0.01$  (see §3.2.2 for experiments that vary  $\Sigma_d/\Sigma_g$ ). Figures 6 and 7 demonstrate this point: the flow for  $Ri = 0.0625$  eventually mixes whereas that for  $Ri = 0.125$  keeps the dust layer intact for as long as  $t_f = 100\Omega_0^{-1}$ . The same Fourier analysis of §3.1, applied to the latter run, reveals no growth of any mode. Repeating the  $Ri = 0.125$  run at higher resolution— $(N_x, N_y, N_z) = (128, 128, 64)$ —confirms these results (run S2a).

### 3.2.1. Sensitivity to Initial Velocity Perturbations

Naturally, reducing the initial velocity perturbations increases the time required for the layer to overturn. The dependence is very slight; lowering the maximum perturbation velocity from  $10^{-3}c_{s0}$  to  $10^{-6}c_{s0}$  increases the time to overturn by  $10\text{--}20\Omega_0^{-1}$  (runs S3a and S4a). (Nonetheless, eliminating the initial perturbations altogether produces no evolution in the shearing box whatsoever.)

The instability grows fastest at “co-rotation,” where  $v_y = 0$ , and spreads radially inward and outward from that location. This behavior is evident in Figure 8, and we observe it in all our unstable runs. Upon removing all initial velocity perturbations in a narrow annulus surrounding co-rotation, and leaving the perturbations in place everywhere else, we find that the flow outside co-rotation still overturns, though more slowly. Eventually the instability spreads to co-rotation and mixes dust uniformly throughout the entire box. This experiment assures us that the instability is not an artifact of  $v_y = 0$ . At present we attribute all this behavior to the fact that our fixed-amplitude initial velocity perturbations are fractionally larger near co-rotation; i.e., the initial perturbation  $\delta v_y \sim 10^{-3}c_{s0}$  is a greater fraction of  $v_y$  near co-rotation than elsewhere. It would therefore be natural to expect the instability to manifest itself most

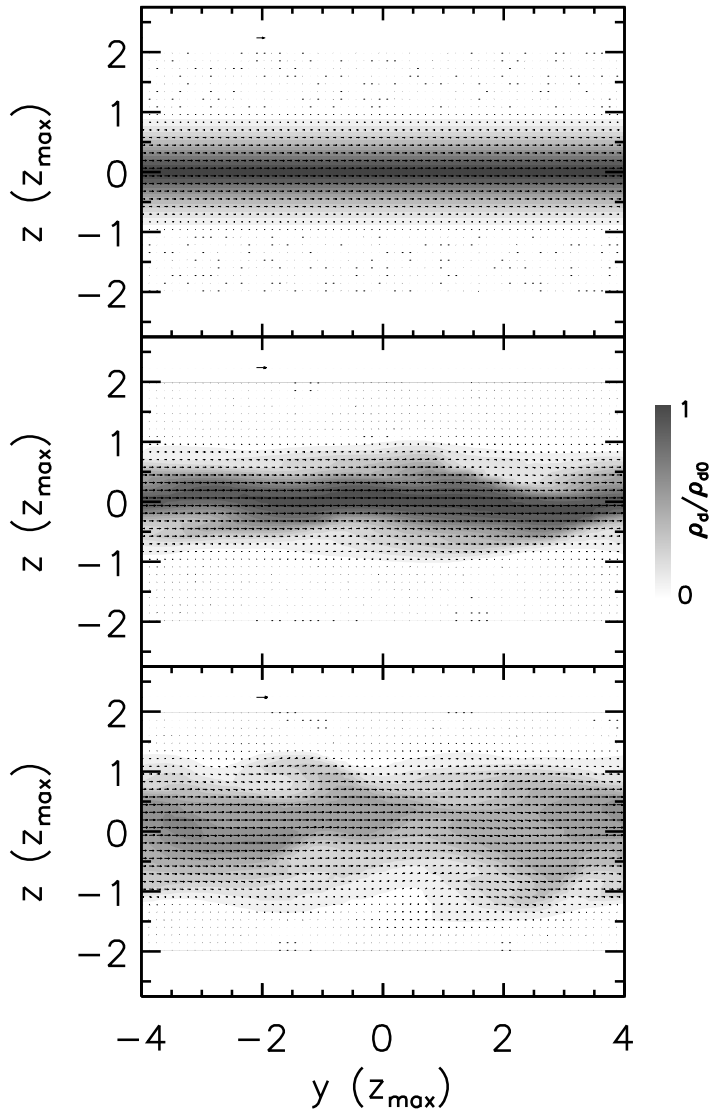


FIG. 6.— Snapshots of the  $(y, z)$  flow, at fixed  $x = 0$ , for  $Ri = 0.0625$  and  $\mu_0 = 1.989$ , in a fully shearing box ( $q = 3/2$ ), at times  $t = 0$  (top),  $t = 24\Omega_0^{-1}$  (middle), and  $t = 37\Omega_0^{-1}$  (bottom). Greyscale denotes the density of dust only, normalized to the density of dust at the midplane at  $t = 0$ . Velocity vectors are shown in the frame rotating with dust-free gas (see top panel). The lone arrow at the top of each panel gives the length of  $v_{\max}$  for that panel only. Data are from simulation S3 for which  $(L_x, L_y, L_z) = (8, 8, 4)z_{\max}$ ,  $(N_x, N_y, N_z) = (64, 64, 32)$ , and  $\Sigma_d/\Sigma_g = 0.01$ .

quickly at co-rotation.

### 3.2.2. Varying the Height-Integrated Metallicity $\Sigma_d/\Sigma_g$

For solar or super-solar values of  $\Sigma_d/\Sigma_g = 0.01$ – $0.05$ , the value of  $Ri_{\text{crit}}$  changes little from 0.1, as runs S5–S8 of Table 2 attest. However,  $Ri_{\text{crit}}$  changes substantially for sub-solar metallicities—it decreases to  $\sim 0.02$  for  $\Sigma_d/\Sigma_g = 0.001$  (runs S9–S12). This result indicates that the Richardson number alone is an inadequate predictor of instability under general circumstances. Still, because sub-solar metallicities seem less relevant for planet formation, we have not pursued the question of what should replace the Richardson criterion, and we content ourselves with citing  $Ri_{\text{crit}} \approx 0.1$  with the understanding that this result applies only for solar and moderately super-solar metallicities.

Values of  $\mu_0$  and  $\Sigma_d/\Sigma_g$  at fixed  $Ri = 0.1 \approx Ri_{\text{crit}}$  are displayed in Figure 9. In a minimum-mass nebula for which  $\Sigma_d/\Sigma_g = 0.01$ ,  $Ri = 0.1$  corresponds to a Toomre  $Q \approx M/[2\pi r^3 \rho_{g0}(1 + \mu_0)] \approx 25$ , independent of disk radius if  $\rho_{g0} \propto r^{-3}$ , as is approximately the case in standard nebular models. Under these conditions, our neglect of the dust layer’s self-gravity is well justified. Only when  $\Sigma_d/\Sigma_g \gtrsim 0.05$  ( $\mu_0 \gtrsim 30$ ; see run S8) does dust self-gravity become important (Sekiya 1998).

### 3.2.3. Baroclinic vs. Kelvin-Helmholtz

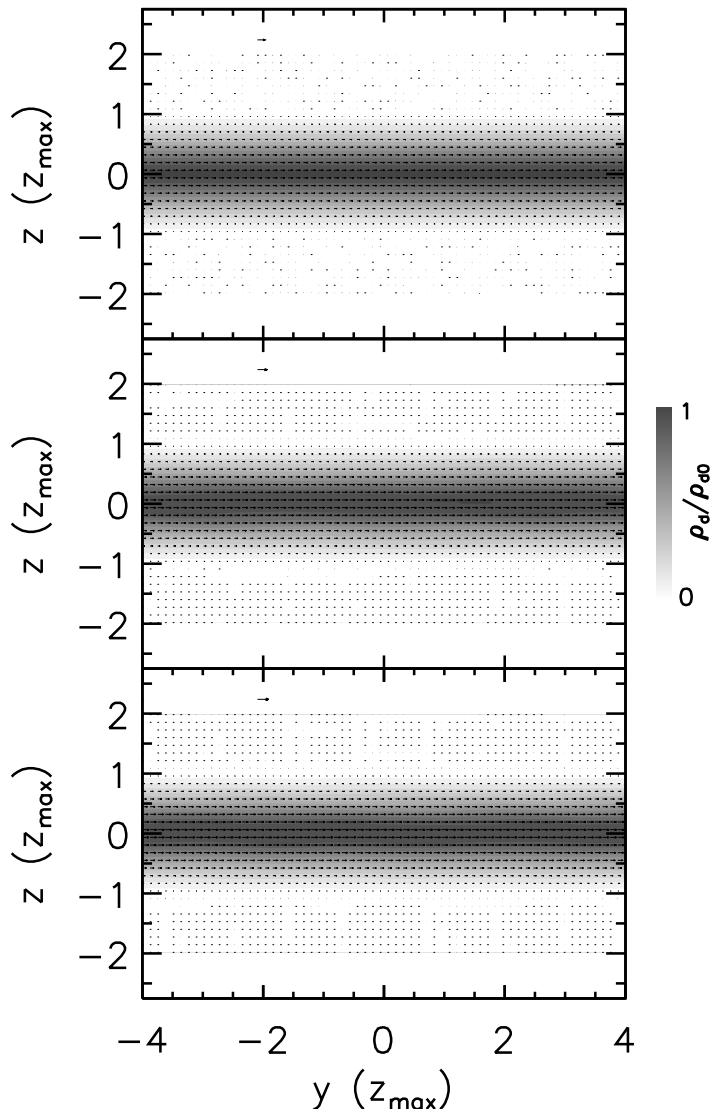


FIG. 7.— Snapshots of the  $(y, z)$  flow, at fixed  $x = 0$ , for  $Ri = 0.125$  and  $\mu_0 = 1.31$ , in a fully shearing box ( $q = 3/2$ ), at times  $t = 0$  (top),  $t = 25\Omega_0^{-1}$  (middle), and  $t = 50\Omega_0^{-1}$  (bottom). Greyscale denotes the density of dust only, normalized to the density of dust at the midplane at  $t = 0$ . Velocity vectors are shown in the frame rotating with dust-free gas (see top panel). The lone arrow at the top of each panel gives the length of  $v_{\max}$  for that panel only. Data are from simulation S2 for which  $(L_x, L_y, L_z) = (8, 8, 4)z_{\max}$ ,  $(N_x, N_y, N_z) = (64, 64, 32)$ , and  $\Sigma_d/\Sigma_g = 0.01$ .

We cannot say whether the observed turnover of the dust layer in a fully shearing disk is better ascribed to the Kelvin-Helmholtz instability (as studied by, e.g., Chandrasekhar 1961) or to the baroclinic instability (as studied by Cabot 1984, Knobloch & Spruit 1986, and Arlt & Urpin 2004). Both instabilities rely on the vertical shear. For  $Ri \approx 0.1$ , the maximum vertical shearing frequency  $\sim \Omega/\sqrt{Ri}$  exceeds, by factors of a few, both the maximum Brunt-Väisälä frequency  $\sim \Omega$  (thereby satisfying the traditional criterion for the KHI) and the rotation frequency  $\Omega$  (thereby satisfying the criterion for “large baroclinity,” as defined by Knobloch & Spruit 1986). An analytic criterion for the baroclinic instability, relevant for non-axisymmetric perturbations, that is valid near the midplane of a radially shearing disk and for arbitrary values of the vertical shear, is not known (Knobloch & Spruit 1986).

#### 4. SUMMARY

We have performed numerical simulations of flows near the dust-rich midplanes of protoplanetary disks. Dust particles are assumed small enough that they are perfectly entrained in gas, and disk self-gravity is neglected. The midplane flow is doubly shearing; the rotational velocity varies with height according to the vertical gradient in dust density, and it also varies with radius according to the usual Keplerian shear. The simulations are necessarily three-dimensional and performed in a shearing box.

Despite the complications introduced by rotation and tidal gravity, the Richardson criterion for the onset of the Kelvin-Helmholtz instability still proves useful for solar to moderately super-solar height-integrated metallicities. Dust

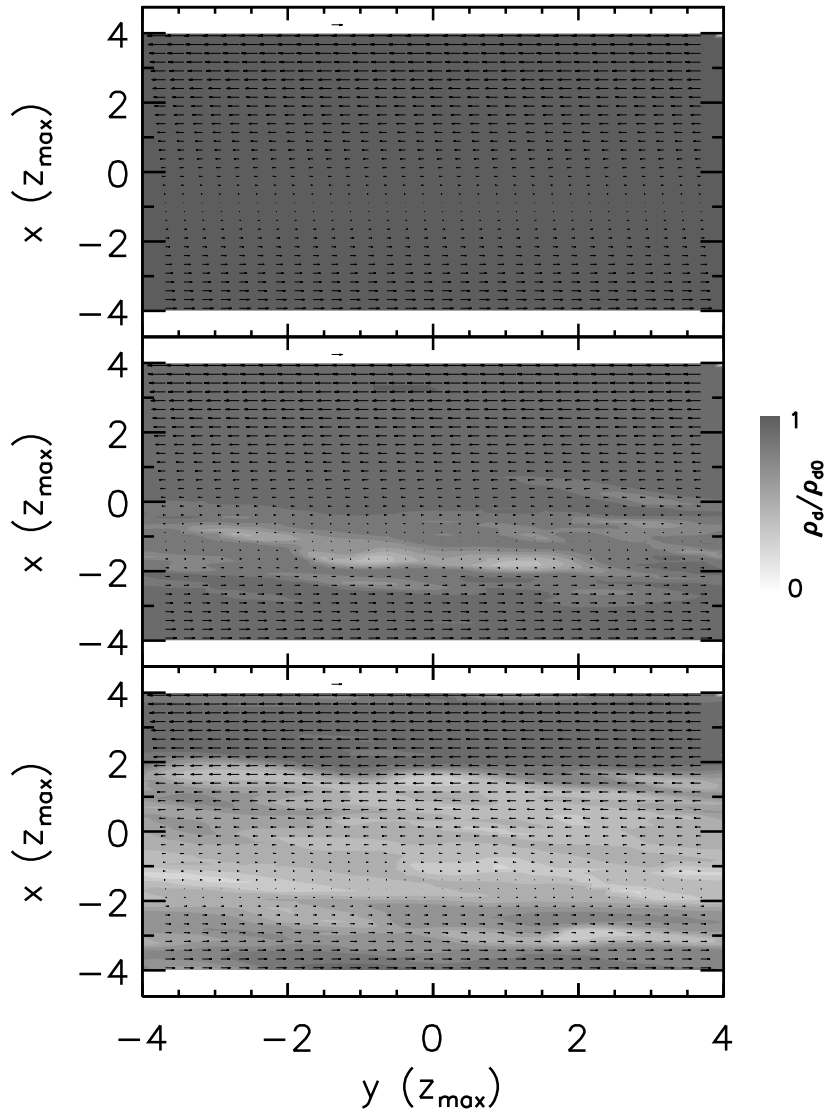


FIG. 8.— Snapshots of the midplane  $(x, y)$  flow, at fixed  $z = 0$ , for  $Ri = 0.0625$  and  $\mu_0 = 1.989$ , in a fully shearing box ( $q = 3/2$ ), at times  $t = 0$  (top),  $t = 24\Omega_0^{-1}$  (middle), and  $t = 37\Omega_0^{-1}$  (bottom). Greyscale denotes the density of dust only, normalized to the density of dust at the midplane at  $t = 0$ . Velocity vectors are shown in the frame rotating at  $\Omega_0$ . Note how  $v_y = 0$  at  $x < 0$ , not at the usual  $x = 0$ , a consequence of the imposed background radial pressure gradient  $(\partial P/\partial r)_{t=0}$  that enforces sub-Keplerian flow. The lone arrow at the top of each panel gives the length of  $v_{\max}$  for that panel only. Data are from simulation S3 for which  $(L_x, L_y, L_z) = (8, 8, 4)z_{\max}$ ,  $(N_x, N_y, N_z) = (64, 64, 32)$ , and  $\Sigma_d/\Sigma_g = 0.01$ .

layers characterized by constant Richardson number and  $\Sigma_d/\Sigma_g \approx 0.01$ – $0.05$  overturn and mix if  $Ri \lesssim 0.1$ , but remain intact at larger  $Ri$ . This result contrasts with the situation when only the Coriolis force is accounted for and the radial shear is suppressed: in that case, unstable modes persist for  $Ri$  as large as 16. But because these “Coriolis-only” (and likely baroclinic; Cabot 1984) modes at large  $Ri$  grow at rates that are substantially slower than the Kepler strain rate of  $3\Omega/2$ , they are stabilized and rendered impotent by the Kepler shear.

In hindsight, our guess (§1) that the critical  $Ri$  dividing stability from instability might only change by a factor of order unity proved correct, though only for solar to moderately super-solar metallicities: we find that  $Ri_{\text{crit}}$  for our doubly shearing flows is about half that of the traditional value of  $1/4$ , if  $\Sigma_d/\Sigma_g \approx 0.01$ – $0.05$ . This is sensible insofar as  $Ri_{\text{crit}} \approx 0.1$  gives a vertical shearing frequency  $\partial v_y/\partial z$  that is a few times faster than any of the other frequencies of the problem: the Brunt-Väisälä frequency for vertical oscillations (this reaches a maximum of  $\sim \Omega$  at  $z \sim z_d$ ), the Kepler strain rate ( $3\Omega/2$ ), and the Coriolis turning frequency ( $2\Omega$ ). Deeper insights, including an understanding of why  $Ri_{\text{crit}} \ll 0.1$  for  $\Sigma_d/\Sigma_g \ll 0.01$ , might be gained by study of the geophysical literature, where doubly shearing, rotating flows are commonplace (see, e.g., Chapter 7 of Pedlosky 1979, which discusses baroclinic instabilities).

We conclude that for a standard, height-integrated, solar metallicity of  $\Sigma_d/\Sigma_g = 0.01$ , the dust density at the midplane can be at most  $\sim 1.5\times$  greater than the gas density. If we assume a gas density appropriate to a minimum-mass disk, then the maximum total density of gas and dust is still too low, by a factor of  $\sim 25$ , for the marginally stable layer to become gravitationally unstable. The literature discusses two remedies. The first is to find ways of enhancing

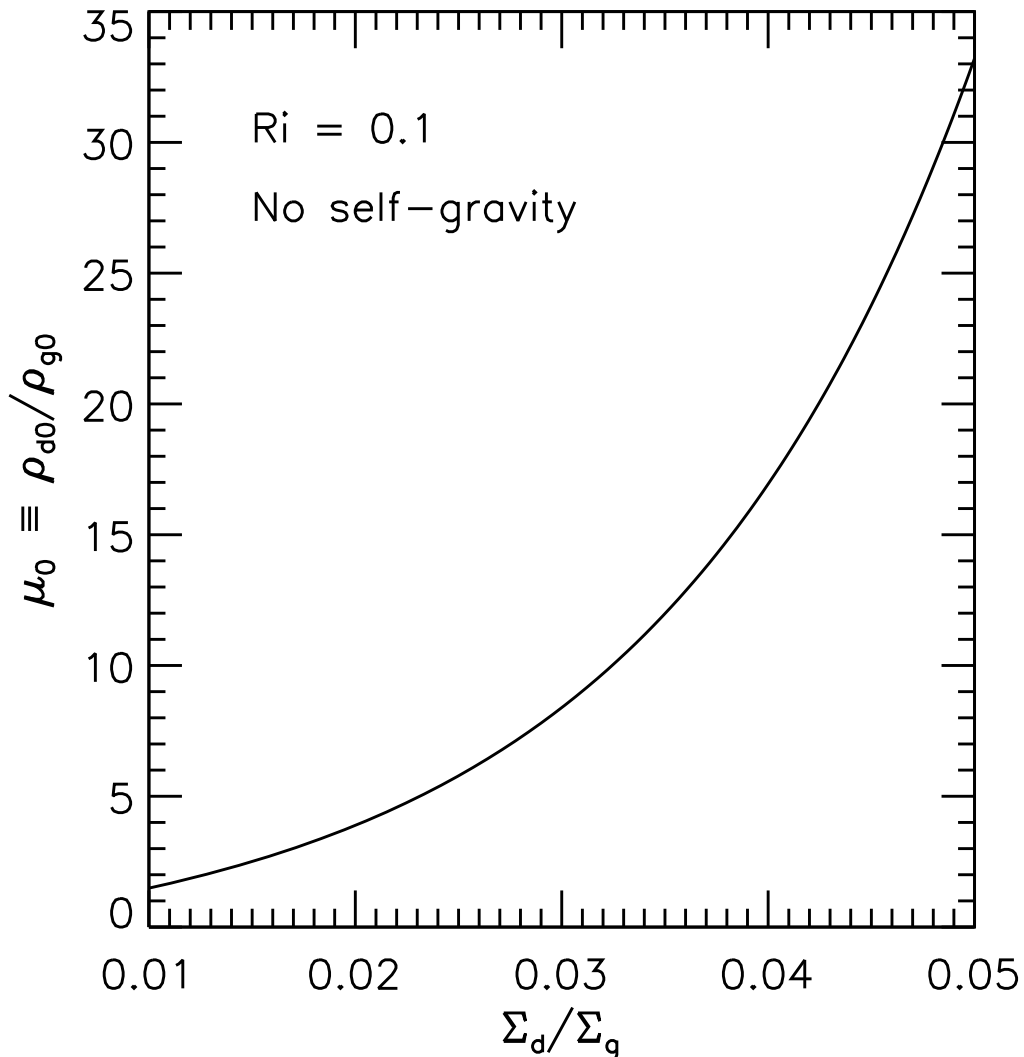


FIG. 9.— One-to-one correspondence between the central concentration  $\mu_0$  and height-integrated metallicity  $\Sigma_d/\Sigma_g$  at fixed  $Ri = 0.1 \approx Ri_{crit}$ . Once the height-integrated metallicity is several times solar, the midplane dust-to-gas density  $(1 + \mu_0)\rho_{g0}$  can approach Roche densities (see §4).

$\Sigma_d/\Sigma_g$  by factors of 3–10, thereby increasing the dust-to-gas ratio at the midplane by factors of  $\sim 30$  at fixed  $Ri = 0.1$  (Sekiya 1998; Youdin & Shu 2002; see also our Figures 3 and 9, and run S8 in Table 2). Possible means of increasing the height-integrated metallicity include (i) decreasing  $\Sigma_g$  through photoevaporation of gas, (ii) increasing  $\Sigma_d$  by radial drift and pile-up of particles (Youdin & Shu 2002; Youdin & Chiang 2004) or (iii) increasing  $\Sigma_d$  by radiation blow-back of grains into the rim of a transitional disk (Chiang & Murray-Clay 2007). Gas giants that form in such a metal-rich environment might be expected to have metallicities enhanced above the solar value by similar factors of 3–10. Indeed some hot Jupiters have remarkably metal-rich interiors (Sato et al. 2005). Alternatively, one can relax the assumption of perfect coupling between dust and gas, and exploit drag instabilities that result from finite momentum stopping times and the backreaction of dust on gas (Youdin & Goodman 2005; Johansen et al. 2007).

We thank Anders Johansen, Bryan Johnson, Eve Ostriker, Jack Wisdom, and Andrew Youdin for helpful discussions. We owe to Jeremy Goodman an insightful referee’s report that brought to light the baroclinic instability. This work was supported by NSF grant AST-0507805.

#### REFERENCES

- |  |   |
|--|---|
| <p>Arlt, R., &amp; Urpin, V. 2004, <i>A&amp;A</i>, 426, 755<br/>           Cabot, W. 1984, <i>ApJ</i>, 277, 806<br/>           Chandrasekhar, S. 1961, <i>Hydrodynamic and Hydromagnetic Stability</i> (New York: Dover)<br/>           Chiang, E.I., et al. 2001, <i>ApJ</i>, 547, 1077</p> | <p>Chiang, E., &amp; Murray-Clay, R. 2007, <i>Nature Physics</i>, 3, 604<br/>           Drazin, P.G., &amp; Reid, W.H. 1981, <i>Hydrodynamic Stability</i> (Cambridge: Cambridge Univ. Press)<br/>           Goldreich, P., &amp; Lynden-Bell, D. 1965, <i>MNRAS</i>, 130, 125<br/>           Goldreich, P., &amp; Ward, W.R. 1973, <i>ApJ</i>, 183, 1051</p> |
|--|---|

- Gómez, G.C., & Ostriker, E.C. 2005, *ApJ*, 630, 1093 (GO)
- Hawley, J.F., Gammie, C.F., & Balbus, S.A. 1995, *ApJ*, 440, 742
- Hayashi, C. 1981, *Prog. Theor. Phys. Suppl.*, 70, 35
- Howard, L.N. 1961, *J. Fluid Mech.*, 10, 509
- Ishitsu, N., & Sekiya, M. 2003, *Icarus*, 165, 181 (IS)
- Johansen, A., Henning, T., & Klahr, H. 2006, *ApJ*, 643, 1219 (JHK)
- Johansen, A., et al. 2007, *Nature*, 448, 1022
- Knobloch, E., & Spruit, H.C. 1986, *A&A*, 166, 359
- Li, L.-X., Goodman, J., & Narayan, R. 2003, *ApJ*, 593, 980
- Miles, J.W. 1961, *J. Fluid Mech.*, 10, 496
- Pedlosky, J. 1979, *Geophysical Fluid Dynamics* (New York: Springer-Verlag)
- Safronov, V.S. 1969, *Evolution of the Protoplanetary Cloud and the Formation of the Earth and Planets* (Moscow: Nauka Press)
- Sato, B., et al. 2005, *ApJ*, 633, 465
- Sekiya, M. 1998, *Icarus*, 133, 298
- Stone, J.M., & Norman, M.L. 1992, *ApJ Supp.*, 80, 753
- Tritton, D.J. 1988, *Physical Fluid Dynamics* (Oxford: Oxford University Press)
- von Neumann, J., & Richtmyer, R.D. 1950, *J. Appl. Phys.*, 21, 232
- Weidenschilling, S.J. 1977, *MNRAS*, 180, 57
- Weidenschilling, S.J. 1980, *Icarus*, 44, 172
- Youdin, A.N., & Chiang, E.I. 2004, *ApJ*, 601, 1109
- Youdin, A.N., & Goodman, J. 2005, *ApJ*, 620, 459
- Youdin, A.N., & Shu, F.H. 2002, *ApJ*, 580, 494